Published in final edited form as:
J Phys Condens Matter. 2010 May 19; 22(19): . doi:10.1088/0953-8984/22/19/194116.

How deeply cells feel: methods for thin gels

Amnon Buxboim[1,2], **Karthikan Rajagopal**[2], **Andre' E.X. Brown**[1,2,*], and **Dennis E. Discher**[2,3]

[1]Department of Physics and Astronomy, University of Pennsylvania, Philadelphia, PA, 19104.

[2]Nano/Bio Interface Center, University of Pennsylvania, Philadelphia, PA, 19104.

[3]Physics and Cell and Molecular Biology Graduate Groups, University of Pennsylvania, Philadelphia, PA, 19104.

Abstract

Tissue cells lack the ability to see or hear but have evolved mechanisms to feel into their surroundings and sense a collective stiffness. A cell can even sense the effective stiffness of rigid objects that are not in direct cellular contact – like the proverbial princess who feels a pea placed beneath soft mattresses. How deeply a cell feels into a matrix can be measured by assessing cell responses on a controlled series of thin and elastic gels that are affixed to a rigid substrate. Gel elasticity E is readily varied with polymer concentrations of now-standard polyacrylamide hydrogels, but to eliminate wrinkling and detachment of thin gels from an underlying glass coverslip, vinyl groups are bonded to the glass before polymerization. Gel thickness is nominally specified using micron-scale beads that act as spacers, but gels swell after polymerization as measured by *z*-section, confocal microscopy of fluorescent gels. Atomic force microscopy (AFM) is used to measure E at gel surfaces, employing stresses and strains that are typically generated by cells and yielding values for E that span a broad range of tissue microenvironments. To illustrate cell sensitivities to a series of thin-to-thick gels, the adhesive spreading of mesenchymal stem cells was measured on gel mimics of a very soft tissue (eg. brain, $E \sim 1$ kPa). Initial results show that cells increasingly respond to the rigidity of an underlying 'hidden' surface starting at about 10–20 μm gel thickness with a characteristic tactile length of less than about 5 μm.

1. Introduction

Cellular microenvironments within different tissues are characterized not only in terms of protein composition and protein-protein interactions but also in terms of the collective properties that emerge such as local elasticity and structure – which tend to be tissue specific. The elasticity of microenviroments within brain(1–2), fat(3), muscle(4–5), cartilage(6) and pre-calcified bone(7–10) ranges over more than two orders of magnitude (Fig. 1A) with key contributions from the most abundant proteins in animals, namely the extracellular matrix (ECM) proteins such as collagens. Cells within tissues constantly probe the mechanical properties of their surroundings by adhering and actively pulling, sensing the resistance to induced deformations. Mechanical signals feed back and regulate cytoskeletal organization and actomyosin contractility – thereby modulating the traction forces that are essential to cellular mechanosensitivity(11). Like a cruise control device for setting car speed or a thermostat that controls air-conditioners and heating devices, the inside ➔ outside ➔ in sensing scheme can control a range of processes, including cell spreading and migration(12), as well as cell stiffness(13) and differentiation(5,8).

*Currently at Division of Cell Biology, MRC Laboratory of Molecular Biology, Hills Road, Cambridge, CB2 0QH.

Many tissues also possess complex anatomies that are not simply described by a single value of elasticity – formally, the Young's modulus *E*. Cartilage, for example, 'feels' stiff when strained with probes that are microns or more in length scale, which is the length scale of the 200 nm diameter collagen fibers, but cartilage appears considerably softer when nano-indenters probe the gelatinous network of glycoprotein that interpenetrate throughout cartilage(6). The macromechanical properties of a fibrous collagen network are necessary for sustaining high external stresses of tissues but are distinct from the properties at the scale of adhesions. Chondrocytes are encased in a microns-thick gelatinous pericellular matrix of E ~25 kPa(14) (Fig. 1B, top) that is embedded in the fibrous collagen cartilage matrix which is at least an order of magnitude stiffer. Such stratified arrangements of soft but thin matrices on top of substrates of distinct elasticity are seen in other tissues and suggest epitaxial growth processes. Within bone, matrix-secreting osteoblast cells adhere to an osteoid matrix of $E \sim 35$ kPa[8] that is microns-thin on top of calcified, rigid bone (Fig. 1B, bottom). In these two examples, cells are likely to sense the collective stiffness of soft thin matrices on top of rigid substrates: soft matrices should be more difficult for cells to deform in such geometries.

Physically well-characterized culture models are needed to address how deeply cells feel and to eventually unravel the related physicochemical signals to cells in various tissues – including mesenchymal tissues such as cartilage or bone. Biomaterial coatings would also benefit from a detailed understanding of thickness-coupled film elasticity effects. Gels should be considered thin when similar to the lateral displacements exerted by cells, and this distance is typically a ~few microns even with cells on thin, wrinkling films of silicone(12). Here we describe our approach for the preparation of firmly attached synthetic polymer matrices of controlled elasticity and thickness (Fig. 1C). We extend the now-standard collagen-coated polyacrylamide (PA) gel systems(12), by first describing a method for strong attachment of thin gels to glass coverslips during gel polymerization. Mechanical properties of both bulk gels and the PA films are then described with measurements of thickness by confocal microscopy and elasticity measurements by AFM. Finally, we present preliminary data for the effects that thin compliant gels have on cells.

2. Chemical functionalization of covalent gel bonding

PA gels are commonly used for elctrophoretic separations of proteins with pore-size adjusted by monomer and crosslinker concentrations, but for more than a decade PA gels have also been functionalized for use in cell culture as *E*-controlled substrates attached to glass slides or coverslips(12). Elasticity is adjusted by varying the concentration of cross-linker while cell adhesion requires attachment of a thin layer of cell-binding ECM proteins such as rat tail-derived type-I collagen(17–18) or matrigel, which is a laminin-based ECM protein mix from mouse tumors,(1) or else other ECM proteins(19). While most past studies have employed such systems as films that are estimated to be 50–100 μm thick, initial studies of thin gel effects (8,20) have paid little attention to effects such as gel detachment.

Cell matrices are not only strained by the contractility of cells but are also subjected to external loads, such as fluid shear stresses in vivo as well as in cell culture – with pipetting during media changes. Most of these mechanical stresses are applied at the cell-matrix interface, and thin gels are significantly more prone to being detached and/or wrinkled(21) than thick films. To achieve an irreversible covalent attachment of PA gels to glass, we first functionalize the glass with allyltrichlorosilane (ATCS) which presents vinyl groups on the surface (Fig. 2A). ATCS-functionalized coverslips are highly hydrophobic as observed by the large contact angle of water droplets on the glass surface and by the tendency of the cover slips to float on water; hydrophobicity of ATCS-treated cover slips thus provides a simple means to confirm surface modification.

The vinyl groups in ACTS will react with acrylamide during the free radical polymerization of PA, whereas the standard method to prepare coverslips uses aminopropyltriethoxysilane-silanized and glutaraldehyde (GA) functionalization in a less direct surface reaction(12). To compare the two methods, an equal volume of PA gel (0.1 mL) was polymerized on each and, after gelation, gels were thoroughly rinsed in water and then immersed in ethanol to stress the film through swelling (Fig. 2B). Within a few minutes in ethanol the gels became white-opaque indicative of gel dehydration, and as a result of the extreme volumetric stresses, the GA-attached gel spontaneously detached from the coverslip – as shown held on a spatula. The ATCS-attached PA gel also resisted detachment when scratched with a spatula, thus indicating firm bonding to the glass coverslip. PA gel attachment to ATCS-treated glass surfaces was also found to sustain extensive immersions and rinsing in methanol and in toluene and gel recovery was observed when returned to water (data not shown).

3. Rheological properties of polyacrylamide gels

To understand gelation within a confined geometry, the elasticity of PA gels was measured with time while polymerizing between the platens of a strain-controlled rheometer. Acrylamide monomer concentration was varied from 3% to 6% w/v with a 100 fold lower cross linker concentration (Fig. 3A), and the polymerization time proved longer for dilute gels than for dense gels as shown by the half-max *E* that are connected by a dashed black line. However, within 15 minutes gel polymerization was essentially complete for all gels, with *E* reaching a final value between 0.26 and 9.9 kPa. This ~38 fold difference was achieved with just 2-fold differences in both monomer and cross linker concentrations, which highlights the general sensitivity of gel mechanics to chemistry. Similar physical principles – and probably more profound subtleties – apply also to natural ECM.

Linearly-elastic and homogeneous elastic solids are mechanically specified by *E* and one other mechanical property such as the Poisson ratio ν, which describes the lateral contraction during axial stretching and relates to compressibility. To determine ν of PA gels, we imaged a cylindrical gel (8% w/v, nominal stiffness of 34 kPa) during a simple tensile test in air(22). Fig. 3B plots the strain-dependent relative width λ_*. Since relative volume is given by (strain + 1) $(\lambda_*)^2$, the width of an incompressible sample will vary as $(\text{strain} + 1)^{-1/2}$. This is the dashed line in Fig. 3B, while the points are data from the PA gel. For incompressible materials, as hydrated PA is seen to be in air, ν = ½ even for very large extensions up to 2.5-fold (= 250% strain). When PA gels are stressed under water and attached to a surface(23), one report gives ν = 0.26 to 0.34 for 0.4% w/v PA gels with 0.05–0.5% cross linker concentration; in contrast, micropipette aspiration measurements of PA gels with E = 7–8 kPa gave ν ~ 0.5.(24) Fig. 3B includes a plot of $(\text{strain} + 1)^{-0.3}$, which is consistent with ν = 0.3 for all strains and which differs by only about 20% from the incompressible case. Such analyses might not be standard for small strain elasticity but they are exact for soft hyperelastic materials(25).

Whereas PA gels are homogeneous and possess remarkably linear mechanical properties that are well characterized by standard rheology and AFM measurements, natural ECMs generally exhibit more complex properties. Fibrous networks of the wound-healing ECM protein fibrin, for example, shows a more dramatic decrease in λ_* upon stretching when compared to even an incompressible material(26). Fibrin gels are crosslinked by an essential blood clotting enzyme, the transglutaminase Factor-XIII, so that stretching leads to stressing of proteins that unfold, expose hydrophobic cores, and associate laterally, expelling water in a hydrophilic to hydrophobic transition. Despite all of this biomolecular complexity, and the potential to even lose water when a gel is extended in air, fibrin gels display a relatively linear stress versus strain relation in extensions up to 100% strain (i.e. a single *E*). PA gels might therefore mimic the mechanical properties of even complex biological matrices reasonably well.

4. Thin gels

Thin PA gels were polymerized while sandwiched between ATCS-functionalized and non-functionalized glass coverslips (Fig. 4A). Each gel was prepared from 4μl of acrylamide plus cross linker at 3.6% and 6% w/v monomer concentration, with nominal elasticities of 1 and 10 kPa (recall Fig. 3A) that mimic the microelasticity of brain(1–2,27) and muscle(4–5) respectively (Fig. 1B). Gel thickness was nominally controlled at the micron scale with 0.5 μm and 1 μm monodispersed silica microspheres, serving as physical spacers between the glasses. Thicker gels were also prepared with no spacer beads. After polymerization, gels were immersed in water for a few hours which allowed for easy detachment of the top coverslip.

Gel thickness was evaluated from *z*-stack fluorescence images obtained by a laser-scanning confocal microscope. To fluorescently label the gels, allylamine was included during polymerization (1% of acrylamide mol/mol); allylamine is a small molecule similar in size to acrylamide and is thus unlikely to modify the mechanical properties of the gels, especially since it is almost completely protonated (NH_3^+) in water (amine pKa = 9.5) while acrylamide remains neutral (amide pKa = 0.5). The calculated mean distance between adjacent charged amine groups is 5.8 nm for 6% w/v gels and 7.3 nm for 3.6% w/v gels; these length scales are both larger than the Debye length (for electrostatic interactions) in physiologically buffered solution. Gels were conjugated with fluorescein-isothiocyanate (FITC) fluorophores that bind via the allylamine-flanking primary amines; FITC conjugation was carried out after gel polymerization and not during gel polymerization to minimize steric alterations to the structure of the gels. FITC possesses a carboxyl group which is negatively charged at neutral pH, and so the charge arguments above apply to the dye as well. Microelasticity measurements below will ultimately validate the expectation that labeling perturbations have negligible effect on gel mechanics. Imaging of the fluorescently labeled gels showed laterally homogeneous fluorescence, consistent with gels of uniform thickness and no obvious cracks or wrinkles to affect cell-matrix interactions.

Cross sections of soft (3.6% w/v) and stiff (6% w/v) gels were obtained by confocal microcopy (Fig. 4B). Gel thickness was obtained for each gel at randomly chosen sites (> 5 sites) using an edge detector (Fig. 4C). Z-stack images of parallel slices with submicron thickness (0.25 – 0.67μm) were scanned slice by slice. Fluorescence intensity as a function of z (scanning window position) was generated by a convolution of the gel intensity profile and the scanning laser window (middle). At a first approximation, which holds true for small numerical aperture objective lenses and for homogeneous objective-sample immersion coupling, the laser intensity has a symmetric squared-sinc profile, gel edges (z_1, z_2) can be easily obtained from the z-derivative (right). This derivative-based edge-detector method for evaluating gel thickness remained valid also for gels with non-rectangular intensity gradients that are shallow as compared with the slopes of the convolution curve at vicinity of the gels edges (Fig. 4D).

To assess the origins of intensity gradients and address photo-bleaching effects, gels were scanned both bottom-up and top-down. The differences between fluorescence profiles that were obtained in opposite directions are illustrated for a thick, soft gel (Fig. 4D). Bottom-up scans in which the top of the gel was exposed to laser excitation during the entire scan prior to being imaged showed ~30% decrease in intensity relative to the glass-gel interface. In the opposite scanning direction, the top of the gel was imaged first and thus underwent minimal bleaching relative to lower sections. In this case, the fluorescence intensity at the top of the gel was only ~10% lower than the gel bottom. Similar fluorescence gradients were obtained for top-to-bottom and for bottom-to-top scans using non-immersion objective lenses as were observed with oil-immersion objective lenses. While both objective lenses reveal a modest non-homogeneous density profile through the gel thickness, the refractive index of air is smaller than the specimen (water) in opposite to oil, thus arguing against the notion that the observed

gradients are optical aberrations. Based on an average of the normalized top-down and bottom-up intensity profiles, gel density decreases monotonically with z, reaching 80% PA density at the top of the gel relative to the bottom (for soft gels). This suggests non-uniform swelling of the gels in water, and the degree of swelling relative to the spacer beads is seen to vary from 1.6 to 12.3 fold (Table 1).

To estimate the effects that the rigid substrate has on the effective stiffness that cells are likely to sense when cultured on thin matrices, the microelasticity of thin PA gels was measured using AFM. The characteristic forces and gel deformations that are exerted by AFM amount to tens-to-hundreds pN and extend over a few microns – which are typical of cell-induced stresses and strains(28). Gel *E* was thus evaluated from the force-indentation relations by fitting to the z-parabolic variant of the classical Hertz model(29) that was adjusted to a spherical cone geometry as a model of a pyramidal tip (Fig. 5A, inset). We assume a Poisson ratio $\nu = 0.5$, in accord with our stretching measurements of PA gels (Fig. 3B). Fitting of force-indentation curves is generally subjected to a choice of the indentation range to be fitted. We find that the evaluation of *E* is highly dependent on the choice, with three regimes corresponding to fitting over increasing indentation regimes that start at gel-tip contact points. Importantly, this contact point was evaluated analytically from the increase in the slope of the force-indentation curve and was verified using the relation between the indentation and the tip deflection in the vicinity of the contact point(30). With increasing range of indentation, *E* decreases sharply, reaches a plateau at ~500 nm and then remains unchanged up to ~1 μm range, above which it increases again. The quality of the fit was quantified by the RMS-deviation from the experimental curve and proves to be minimal in the middle regime of the fitting range (Fig. 5B). We find that the patterns described here for the fitting of E and for the RMS-deviation of the fit from the experimental curve were both consistent for all gels with varying nominal elasticity and thickness. We therefore estimated the apparent gel elasticity in the middle regime which satisfies two requirements: (*i*) the fitted *E* is robust to changes in the fitting range, and (*ii*) the mean root-mean-square deviation of the fit from the experimental data per data point is minimal. Both of these conditions are satisfied in figure 5A and in figure 5B respectively for the fit range that is illustrated by green brackets.

The apparent elasticity measured for thin gels differed from expected values, both for 1 and 10 kPa gel formulations (Fig. 5C). Thin gels proved to be softer than bulk gels consistent with swelling and density thinning at the top of the gels (Fig. 4 and Table 1). The effects of the bottom surface on the apparent elasticity of the gels are likely reflected in the increased stiffness of the thinnest gels as compared with the intermediate thickness and thick gels.

To summarize, we present thin PA gels of soft and stiff elasticity and of controlled thickness that range from a few microns to ~10 μm and ~20 μm as nominally set by spacer beads or by limiting volume of the gel precursor. Despite their hydrophobicity, uniform films are formed on the ATCS-derivatized glass substrates onto which the gels bind covalently. Variations in gel thickness and in local micro-elasticity were assessed with AFM measurements at 7–10 randomly chosen sites per gel and for gel duplicates and are presented by the error bars shown in figure 5C. While trends in gel thickness as a function of spacer size and/or gel precursor volume are conserved, gel thickness measurements should be carried out separately for each experiment to obtain absolute values. We find also that the type and brand of glass used both as gel substrates and as overlying coverslips may alter gel thickness even when the same spacer beads are used, so that careful measurement of these systems is probably wise.

Mechanical properties of PA gels are determined at first order by the polymer-to-crosslinker ratio and are related to pore size. Pore sizes in PA gels are typically tens of nanometers and are thus well below the various length scales of relevance, including gel thickness, cell spread area and focal adhesion size. The thin gel are therefore continuous substrata with well defined

elasticity. Confocal images suggest a surface roughness of thin gels is ~0.5 μm (not shown) and within 100-by-100 μm^2 fields of view irregularities of 1–2 μm height are rare. Only for the thinnest gels here is such roughness non-negligible and likely to give rise to an increased variability in gel micro-elasticity (per figure 5). However, over surface areas that correspond to either the area of spread cells (>1000 μm^2) or the area of focal adhesions (~1–10 μm^2), the characteristic roughness of the gel surfaces seems unimportant. Taken together, thin PA gel films seem well defined in terms of structure and effective micro-elasticity, which are both necessary and sufficient for describing the mechanical interactions between surface-immobilized compliant matrices of finite thickness and adhesive and contractile cells.

5. How deeply do cells feel?

To illustrate that the methods described in this paper for the preparation of thin collagen-coated PA gels can be used as cellular matrices with controlled thickness and elasticity and to determine the effects that matrix thickness has on cells, we chose the softest gels for a proof-of-principle study. Mesenchymal stem cells (MSCs, passage 5) can be considered prototypical adhesive mesenchymal cells with mechanosensitivity in terms of spreading and cytoskeleton among other responses(8,31). Gels of nominal $E \sim 1$ kPa and varying thickness were coated with rat-tail type-I collagen (see Methods), and MSCs were plated and cultured for 24 hrs. This is 2–3 times longer than the spreading time constant for these cells on such gels. After 24 hrs, cells were fixed and the cytoskeleton was stained for actin and DNA stained with Hoechst (Fig. 6A). Cells that were cultured on the thinnest gels clearly showed increased spread area relative to thicker gels.

The cell spread area was measured for a large number of randomly selected cells (n~100), and the mean area was indeed seen to decrease with gel thickness from thin (~few microns), to intermediate (~10μ) to thick (~100 μm) gels (Fig. 6B). Maximal spreading of the cells was obtained with stiff and thick gels having the same collagen-coated surface chemistry (nominally 34 kPa); cell morphology has been shown previously to be similar for MSCs that are cultured on osteoid-like 34 kPa gels and glass(8,31). Cells spread area as a function of gel thickness fitted a hyperbolic relationship better than an exponential curve. The hyperbolic fit used here is similar in form to the dependence of the mean interfacial displacement for thin gels that was predicted using finite element computations(31). A threshold thickness that marks the distance that cells feel into compliant homogeneous gels can thus be estimated based on the length scale of the hyperbolic fit. In the case of these ‘soft’as-brain’ gels and in terms of spread area of cells, MSCs certainly sense a rigid surface less than 5 μm beneath them, establishing a tactile length scale, with a more modest response seen already at 10–20 μm.

6. Discussion

To elucidate how deeply cells feel, a model system was developed here consisting of a thin and soft flat matrix affixed to an underlying rigid substrate. The length scale that defines the mechanosensitivity of tissue cells is thus estimated as the threshold matrix thickness below which cells respond not only to the ‘softness’ of the matrix but also to the rigidity of the underlying substrate. Experimentally, thin matrices with controlled elasticity have been fabricated using hydrogels(8) or elastomers(32). In one approach for controlling matrix thickness, soft matrices were polymerized within a linear wedge configuration. The linear wedge geometry establishes a relation between the lateral position and the local matrix thickness, and was reported to enable thickness resolution down to ~5μm(33). Linear wedge matrices continuously scan a range of matrix thickness within each sample, but the regions that correspond to a certain thickness range is limited. Alternatively, rigid monodispersed microspheres were also utilized as spacers for specifying the thickness of hydrogels(28), however the thickness was not directly measured for substrates formed with different spacer

diameters. We show that PA hydrogels undergo significant swelling after being completely polymerized within narrow spaces. Gel swelling hinders the fabrication of very thin submicron hydrogel matrices and also gives rise to a density gradient through the gel. The decrease in gel density with increasing distance from the bottom substrate is likely to give rise to inconsistent gel μ-elasticity through the matrix, and thus could trigger a complex cellular response. In comparison to hydrogels, hydrohpbic elastomers such as polydimethylsiloxane (PDMS) are not likely to undergo significant swelling and are thus advantageous for preparing thin cellular matrices, but the elasticity of such elastomers is very difficult to it control even though it has been reported that reducing the crosslinker-to-monomer molar ratio can generate a substrate elasticity as low as ~5 kPa(32–33). Moreover, soft PDMS matrices tend to become stickier than stiff elastomers and thus not only limit the measurement of μ-elasticity by AFM but also have unclear effects on protein adsorption and cell adhesion.

Cytoskeleton organization and cell morphology are the first phenotypic response of tissue cells to matrix elasticity. Within just a few hours in culture, MSCs form adhesion contacts and spread, reaching maximal spreading in much less than a day(8). In general, tissue cells become more contractile and spread more on stiffer substrates(13,18). A similar increase in cell spread area as observed for matrices with increasing stiffness was also shown for certain types of tissue cells to decreasing thickness on gels with a sufficiently soft bulk gel elasticity. The first study that examined the effects of thin, elastic matrices on cells was done with smooth muscle cells (another mesenchymal cell type) and showed no statistically significant affect on cell spread area on 1 kPa gels that were nominally 5 μm thick as set by 5 μm spacer beads(28). Such gels probably swelled somewhat, perhaps 1.6 fold or more (Table 1), and so the cited results are likely consistent with those here. Subsequent studies with smaller spacer beads indeed suggested cells, notably MSCs, do spread more on soft gels (<10 kPa) with micron-scale thickness as compared with thick ~100 μm gels(8); a similar response to matrix thickness was also reported recently for fibroblasts(34). In the latter study, active mechnosensitivity – referring to cells that actively apply traction forces to probe their surroundings – was analyzed based on Yue's solution for the elastostatic response of compliant structures of multilayered geometries to surface tractions(35) and applied to cellinduced deformation within flat substrates of finite thickness (33–34). Based on such models, the distances that cells are capable of sensing were estimated to be 1.5–2 μm by considering individual micron-scale cell-matrix contacts(34) while traction forces generated at the cell-scale predicted that cells can sense tens of microns away(33). The complexity involved in cells' response to compliant matrices with varying thickness and elasticity was studied using mean field finite element computations in which different cell types were also modeled(31). The distribution of strains at the cell-matrix interface was significantly modified within soft substrates below 2–3 μm thickness by the underlying rigid surface which defines no-slip boundary conditions at the bottom of the gel. Our ACTS bonding to glass helps to enforce such boundary conditions.

Our platform methodology here suggests a threshold thickness 3.4 μm for how deeply MSCs feel into a matrix that is similar in softness to brain tissue. Active mechanosensing of MSCs on fibrin matrices over lateral distances similar to cell sizes(36) exceed our estimations for depth sensing, but we speculate that such fibers slip and/or slide on the gel substrates so that stresses and strains – in such a case – do not propagate significantly into the depth of the substrates. With tighter adhesive compling, physical deformations that are generated at the cellmatrix interface propagate into compliant matrices and decay as the inverse of the distance from the cell. Despite this relatively slow decay, our experiments and others indicate that cellular mechanosensitivity extends only over intermediate length scales that are not much longer than cell-matrix adhesion contacts and certainly much smaller than cell dimensions. The relationships to the spatial distribution of cell-matrix contacts and cytoskeleton organization clearly need to be elucidated.

Methods

Glass substrates treatment

Glass cover slips (thickness #2, Fisher Scientific) were boiled in ethanol for 10 min, rinsed in distilled water (DW) and immersed in RCA at 80°C for 10 min. RCA consists of DW, hydrogen peroxide (30%, Fisher Scientific) and ammonium hydroxide (30%, Fisher Scientific) at 3:1:1 volume ratios. RCA-treated substrates were rinsed in DW, ethanol and chloroform and silanized in 0.1% allyltrichlorosilane (ATCS, Aldrich) in chloroform (Fisher Scientific) with 0.1% triethylaminde (TEA, Fisher Scientific) for 30 min. Coverslips were subsequently rinsed in chloroform, ethanol and DW. ATCS silanization was verified by surface hydrophobicity. Control coverslips were cleaned similarly in RCA and silanized with 1% aminopropyltriethoxysilane (APTES, Sigma) and 1% TEA for one hour in toluene (Fisher Scientific), and functionalized by 0.5% gluteraldehyde (GA, 50% grade-I, Aldrich) in PBS for 30 min. Top glass coverslips (25mm diameter) were boiled in ethanol and RCA-treated as described above. Cleaned coverslips were kept in DW before use.

PA gel preparation

Precursor mixtures of PA gels were made from acrylamide (40%, Sigma), N,N'-methylenebisacrylamide (1.5% w/v bis-AA in DW, Sigma) +/− allylamine (AlAm, Acros Organics) in DW. Acrylamide concentration was varied between 3% and 6% w/v with 1:93 fold bis-AA crosslinker +/− 1:100 AlAm molar concentration ratios. Silica monodispersed microsphere spacers (Thermo Scientific), 0.5 and 1 μm diameter, were added at 0.01% and 0.0023% w/v, which corresponds to 100μm mean lateral inter-bead distance. Gelation was accelerated by 0.1% v/v tetramethylethylenediamine (TEMED, Sigma) and initiated using 0.1% w/v ammonium persulfate (Sigma). Fluorescein isothiocyanate (FITC Isomer-I, Invitrogen) labeling of fully polymerized PA/AlAm gels was carried out in water overnight at 4°c with large excess of fluorophore. Gels for cell culture were further coated with type-I rat tail collagen (BD Biosciences) as follows: Sulfo-Sanpah (Fisher Scientific) was dissolved in 50mM, pH 8 HEPES and pipetted to form a complete coverage on the gels. Gels were placed inside a UV chamber (specimens were placed ~20mm from Spectroline-15A light source) and shined for 10min by 365nm illumination. To minimize fibers formation, collagen was first mixed in equal volume of 4°C 0.1M acetic acid (Fisher Scientific) and then diluted ~20 folds in 4°C 50mM, pH 8 HEPES to a final concentration 0.2mg/ml. To avoid the formation of thick layers of collagen on thin gels, aggregated collagen fibers were separated from non-aggregated fibrils by spinning down at 5000 rpm for 4min (Fisher Scientific, Centrific centrifuge with rotor for twelve 15ml tubes) and collecting only the supernatant for gel coating. Absorbance measurement indicated that 15–20% of the collagen was recovered. Collagen was incubated on the gels while agitated overnight at 37°C. Prior to seeding cells, gels were UV-sterilized (cell culture hood UV light source) for two hours. Gels were kept hydrated during all preparation steps.

Gel rheology

PA gel elasticity was measured with time using a strain-controlled rheometer (TA instruments, RFS-II). A flat titanium plate, 25mm diameter, was used with 0.5ml sample volume and 0.95mm gap. Platform surface temperature was set to 25°c, with 0.1% strain and 1 rad/sec rate.

PA gel stretching

PA gel cylinders (nominally 34kPa, 8% w/v acrylamide and 0.3% w/v bis-AA) were polymerized in ~4 mm diameter syringe tubes (BD syringe). These gels were removed from the syringe and sand was used to create fiducial marks along the sample. Movies were taken during stretching and the longitudinal strain and width were determined using NIH ImageJ

from the relative change in position of the fiducial marks. The relative width was the average of the width determined at a fiducial mark and at a clean region between the fiducial marks.

Gel cross-section

Cross section images of FITC-labeled PA/AlAm gels were acquired by confocal microscope (FV1000, Olympus) using 60X oil-immersion objective (to be added). Pinhole size varied between 100 to 250 μm with 0.25–0.76 μoptimal slice gap. Gel thickness was evaluated using Matlab (Mathworks Inc.) as described in the main text.

Apparent μ-elasticity of thin gels

Force-indentation curves were obtained by AFM (MFP-3D Asylum Research) using pyramidal tip cantilevers (k_{sp} ~ 24 pN/nm, TR400PB, Olympus). Force-indentation data was exported to Matlab for computing the μ-elasticity.

Cell culture

Human mesenchymal stem cells (MSCs, Osiris Therapeutics; Baltimore, MD) were cultured in normal growth media (Low Glucose DMEM (Gibco) + 10% FBS (Sigma) + 1% penicillin/Streptomycin). Cells were plated on the gels (passage 5 after four days of cultivation) at 500 cells/cm^2. Cells on thin gels were fixed in formaldehyde (Fisher Scientific) and stained for F-actin (phalloidin, Sigma), immune-labeled against vinculin (Sigma) and nucleus-stained with Hoechst (Molecular Probes). Fluorescently labeled cells were imaged using an upright microscope (IX71, Olympus) and cell statistics was obtained by Matlab image processing tools.

Acknowledgments

NIH, NSF, NSF-MRSEC, and NSEF-NSEC funding are all gratefully acknoweldeged.

References

1. Flanagan LA, Ju YE, Marg B, Osterfield M, Janmey PA. Neurite branching on deformable substrates. Neuroreport 2002 Dec 20;13(18):2411–2415. [PubMed: 12499839]
2. Georges PC, Miller WJ, Meaney DF, Sawyer ES, Janmey PA. Matrices with compliance comparable to that of brain tissue select neuronal over glial growth in mixed cortical cultures. Biophysical Journal 2006 Apr;90(8):3012–3018. [PubMed: 16461391]
3. Patel PN, Smith CK, Patrick CW. Rheological and recovery properties of poly(ethylene glycol) diacrylate hydrogels and human adipose tissue. Journal of Biomedical Materials Research Part A 2005 Jun 1;73A(3):313–319. [PubMed: 15834933]
4. Ferrari G, Cusella-De Angelis G, Coletta M, Paolucci E, Stornaiuolo A, Cossu G, et al. Muscle regeneration by bone marrow derived myogenic progenitors. Science 1998 Mar 6;279(5356):1528–1530. [PubMed: 9488650]
5. Engler AJ, Griffin MA, Sen S, Bonnetnann CG, Sweeney HL, Discher DE. Myotubes differentiate optimally on substrates with tissue-like stiffness: pathological implications for soft or stiff microenvironments. Journal of Cell Biology 2004 Sep 13;166(6):877–887. [PubMed: 15364962]
6. Stolz M, Raiteri R, Daniels AU, VanLandingham MR, Baschong W, Aebi U. Dynamic elastic modulus of porcine articular cartilage determined at two different levels of tissue organization by indentation-type atomic force microscopy. Biophysical Journal 2004 May;86(5):3269–3283. [PubMed: 15111440]
7. Andrades JA, Santamaria JA, Nimni ME, Becerra J. Selection and amplification of a bone marrow cell population and its induction to the chondro-osteogenic lineage by rhOP-1: an in vitro and in vivo study. International Journal of Developmental Biology 2001 Jun;45(4):689–693. [PubMed: 11461007]
8. Engler AJ, Sen S, Sweeney HL, Discher DE. Matrix elasticity directs stem cell lineage specification. Cell 2006 Aug 25;126(4):677–689. [PubMed: 16923388]

9. Holmbeck K, Bianco P, Caterina J, Yamada S, Kromer M, Kuznetsov SA, et al. MT1-MMP-deficient mice develop dwarfism, osteopenia, arthritis, and connective tissue disease due to inadequate collagen turnover. Cell 1999 Oct 1;99(1):81–92. [PubMed: 10520996]
10. Morinobu M, Ishijima M, Rittling SR, Tsuji K, Yamamoto H, Nifuji A, et al. Osteopontin expression in osteoblasts and osteocytes during bone formation under mechanical stress in the calvarial suture in vivo. Journal of Bone and Mineral Research 2003 Sep;18(9):1706–1715. [PubMed: 12968681]
11. Discher DE, Janmey P, Wang YL. Tissue cells feel and respond to the stiffness of their substrate. Science 2005 Nov 18;310(5751):1139–1143. [PubMed: 16293750]
12. Pelham RJ, Wang YL. Cell locomotion and focal adhesions are regulated by substrate flexibility. Proceedings of the National Academy of Sciences of the United States of America 1997 Dec 9;94 (25):13661–13665. [PubMed: 9391082]
13. Solon J, Levental I, Sengupta K, Georges PC, Janmey PA. Fibroblast adaptation and stiffness matching to soft elastic substrates. Biophysical Journal 2007 Dec 15;93(12):4453–4461. [PubMed: 18045965]
14. Guilak F, Alexopoulos LG, Haider MA, Ting-Beall HP, Setton LA. Zonal uniformity in mechanical properties of the chondrocyte pericellular matrix: Micropipette aspiration of canine chondrons isolated by cartilage homogenization. Annals of Biomedical Engineering 2005 Oct;33(10):1312–1318. [PubMed: 16240080]
15. Sodek J, McKee MD. Molecular and cellular biology of alveolar bone. Periodontology 2000 2000;24:99–126. [PubMed: 11276877]
16. Poole CA, Flint MH, Beaumont BW. Chondrons in Cartilage - Ultrastructural Analysis of the Pericellular Microenvironment in Adult Human Articular Cartilages. Journal of Orthopaedic Research 1987;5(4):509–522. [PubMed: 3681525]
17. Gaudet C, Marganski WA, Kim S, Brown CT, Gunderia V, Dembo M, et al. Influence of type I collagen surface density on fibroblast spreading, motility, and contractility. Biophysical Journal 2003 Nov 1;85(5):3329–3335. [PubMed: 14581234]
18. Engler A, Bacakova L, Newman C, Hategan A, Griffin M, Discher D. Substrate compliance versus ligand density in cell on gel responses. Biophysical Journal 2004 Jan;86(1):617–628. [PubMed: 14695306]
19. Rowlands AS, George PA, Cooper-White JJ. Directing osteogenic and myogenic differentiation of MSCs: interplay of stiffness and adhesive ligand presentation. American Journal of Physiology-Cell Physiology 2008 Oct;295(4):C1037–C1044. [PubMed: 18753317]
20. Buxboim A, Ivanovska IL, Discher DE. Matrix elasticity, cytoskeletal forces and physics of the nucleus: how deeply do cells ‘feel’ outside and in? Journal of Cell Science. accepted.
21. Harris AK, Wild P, Stopak D. Silicone-Rubber Substrata - New Wrinkle in the Study of Cell Locomotion. Science 1980;208(4440):177–179. [PubMed: 6987736]
22. Cesa CM, Kirchgessner N, Mayer D, Schwarz US, Hoffmann B, Merkel R. Micropatterned silicone elastomer substrates for high resolution analysis of cellular force patterns. Rev Sci Instrum 2007 Mar; 78(3)
23. Li Y, Hu ZB, Li CF. New Method for Measuring Poisson Ratio in Polymer Gels. Journal of Applied Polymer Science 1993 Nov 10;50(6):1107–1111.
24. Boudou T, Ohayon J, Arntz Y, Finet G, Picart C, Tracqui P. An extended modeling of the micropipette aspiration experiment for the characterization of the Young's modulus and Poisson's ratio of adherent thin biological samples: Numerical and experimental studies. Journal of Biomechanics 2006;39(9): 1677–1685. [PubMed: 15978599]
25. Beatty FM, Stalnaker DO. The Poisson Function of Finite Elasticity. Journal of Applied Mechanics 1985;53(4)
26. Brown AEX, Litvinov RI, Discher DE, Purohit PK, Weisel JW. Multiscale Mechanics of Fibrin Polymer: Gel Stretching with Protein Unfolding and Loss of Water. Science 2009;325:741–744. [PubMed: 19661428]
27. Kondo T, Johnson SA, Yoder MC, Romand R, Hashino E. Sonic hedgehog and retinoic acid synergistically promote sensory fate specification from bone marrow-derived pluripotent stem cells. Proceedings of the National Academy of Sciences of the United States of America 2005 Mar 29;102 (13):4789–4794. [PubMed: 15778294]

28. Engler AJ, Richert L, Wong JY, Picart C, Discher DE. Surface probe measurements of the elasticity of sectioned tissue, thin gels and polyelectrolyte multilayer films: Correlations between substrate stiffness and cell adhesion. Surface Science 2004 Oct 10;570(1–2):142–154.

29. Hertz H. Über die Berührung fester elastischer Körper. Jounal für die Reine und Angewandte Mathematik 1882;82:156–171.

30. Domke J, Radmacher M. Measuring the elastic properties of thin polymer films with the atomic force microscope. Langmuir 1998;14:3320–3325.

31. Sen S, Engler AJ, Discher DE. Matrix Strains Induced by Cells: Computing How Far Cells Can Fell. Cellular and Molecular Bioengineering 2009;2(1):39–48.

32. Balaban NQ, Schwarz US, Riveline D, Goichberg P, Tzur G, Sabanay I, et al. Force and focal adhesion assembly: a close relationship studied using elastic micropatterned substrates. Nature Cell Biology 2001 May;3(5):466–472.

33. Merkel R, Kirchgebner N, Cesa CM, Hoffmann B. Cell force Microscopy on elastic layers of finite thickness. Biophysical Journal 2007 Nov;93(9):3314–3323. [PubMed: 17660320]

34. Maloney JM, Walton EB, Bruce CM, Vliet KJ. Influence of finite thickness and stiffness on cellular adhesion-induced deformation of compliant substrata. Physical Review E 2008 Oct;78(4)

35. Yue ZQ. On elastostatics of multilayered solids subjected to general surface traction. Q J Mech Appl Math 1996 Aug;49:471–499.

36. Winer JP, Oake S, Janmey PA. Non-Linear Elasticity of Extracellular Matrices Enables Contractile Cells to Communicate Local Position and Orientation. Plos One 2009;4(7)

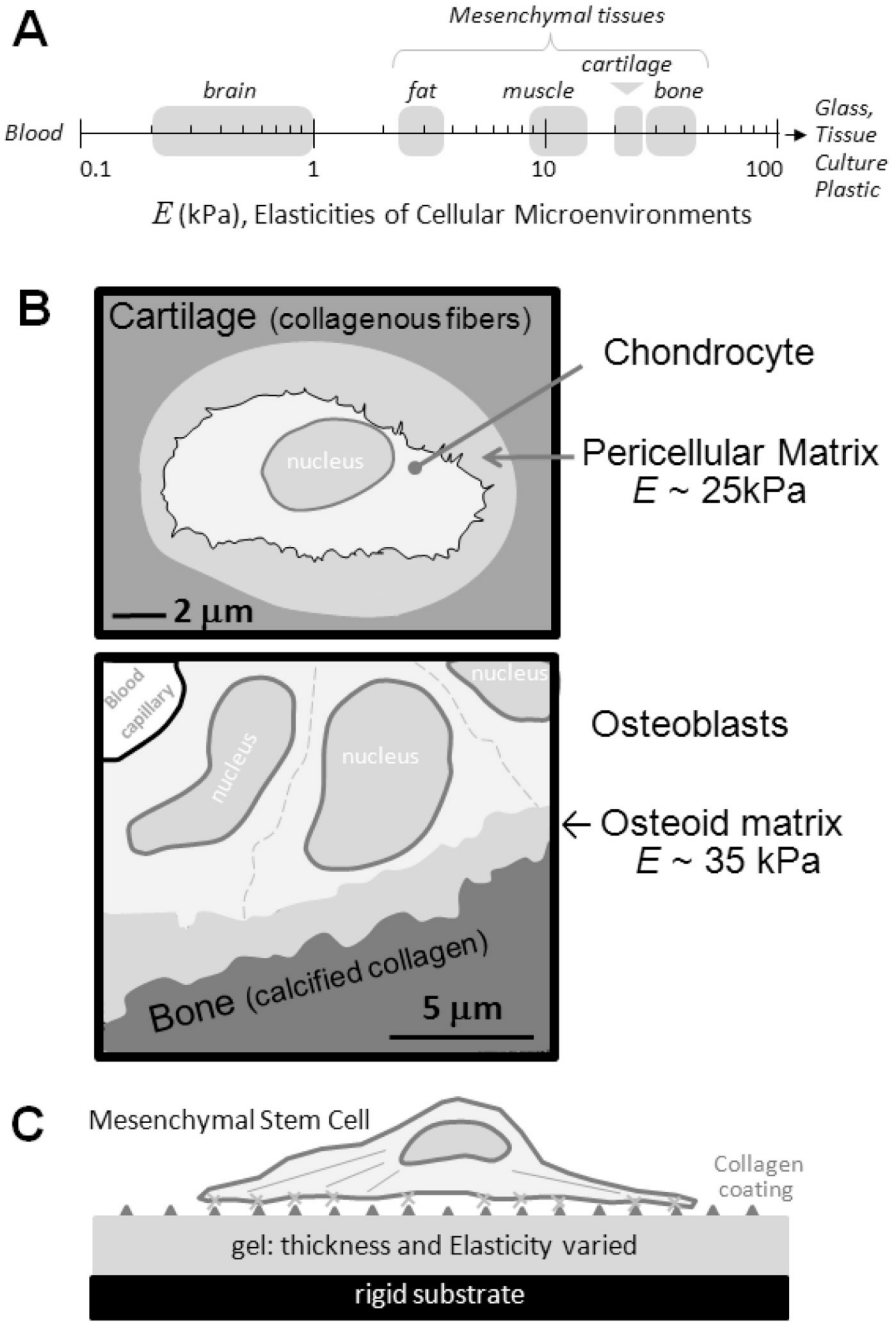

Figure 1.

Tissue microenvironments and models. (A) Cellular microenvironments within tissues are characterized by their elasticity *E*, which ranges over two decades. (B) Anatomically correct, re-traced schematics of mesenchymal microenvironments(15–16). Within cartilage (top), chondron units consist of chondrocytes that are embedded within a pericelluler matrix surrounded by a stiff collagenous matrix. Bone-generating osteoblasts (bottom) adhere to a thin and compliant osteoid ECM that is layered on top of rigid calcified bone. (C) Heterogeneous culture models in which a thin and soft matrix is affixed to a rigid substrate.

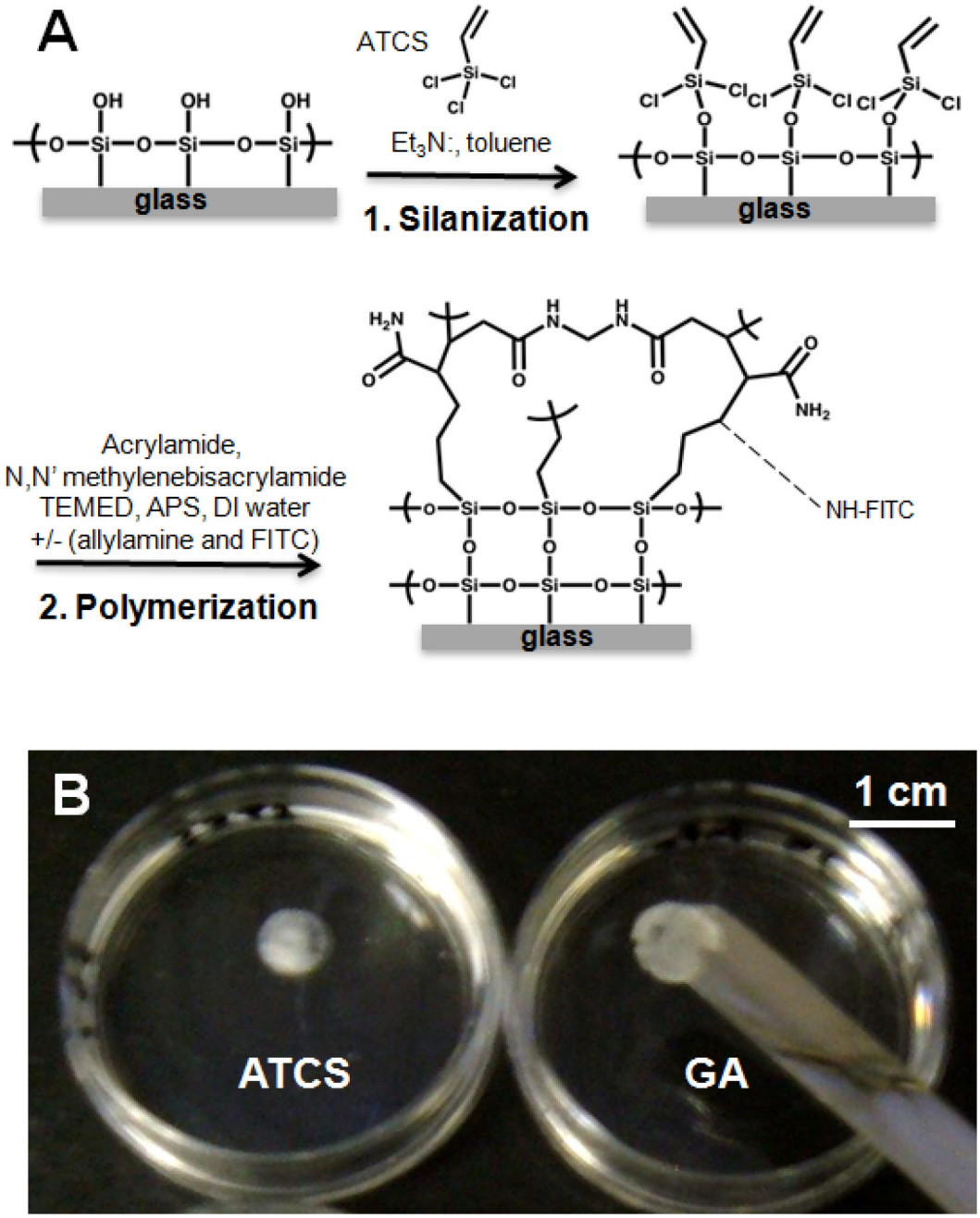

Figure 2.

Surface functionalization of glass substrates for covalent binding of polyacrylamide gels. (A) (1) Cleaned glass substrates (see methods) were silanized with allyltrichlorosilane (ATCS) that forms a dense layer of surface vinyl groups. Covalent attachment of thin polyacrylamide (PA) gels is achieved by direct gel polymerization (2). (B) Irreversible gel attachment to an ATCS treated glass substrate was functionally tested by immersion in ethanol (leading to opaque films) and comparing to a gel that was attached by the standard gluteraldehyde method (GA) (12). Within 30 min, gel detached from GA-treated substrate and is held on a spatula, while the ATCS-immobilized gels remained attached and proved scratch resistant.

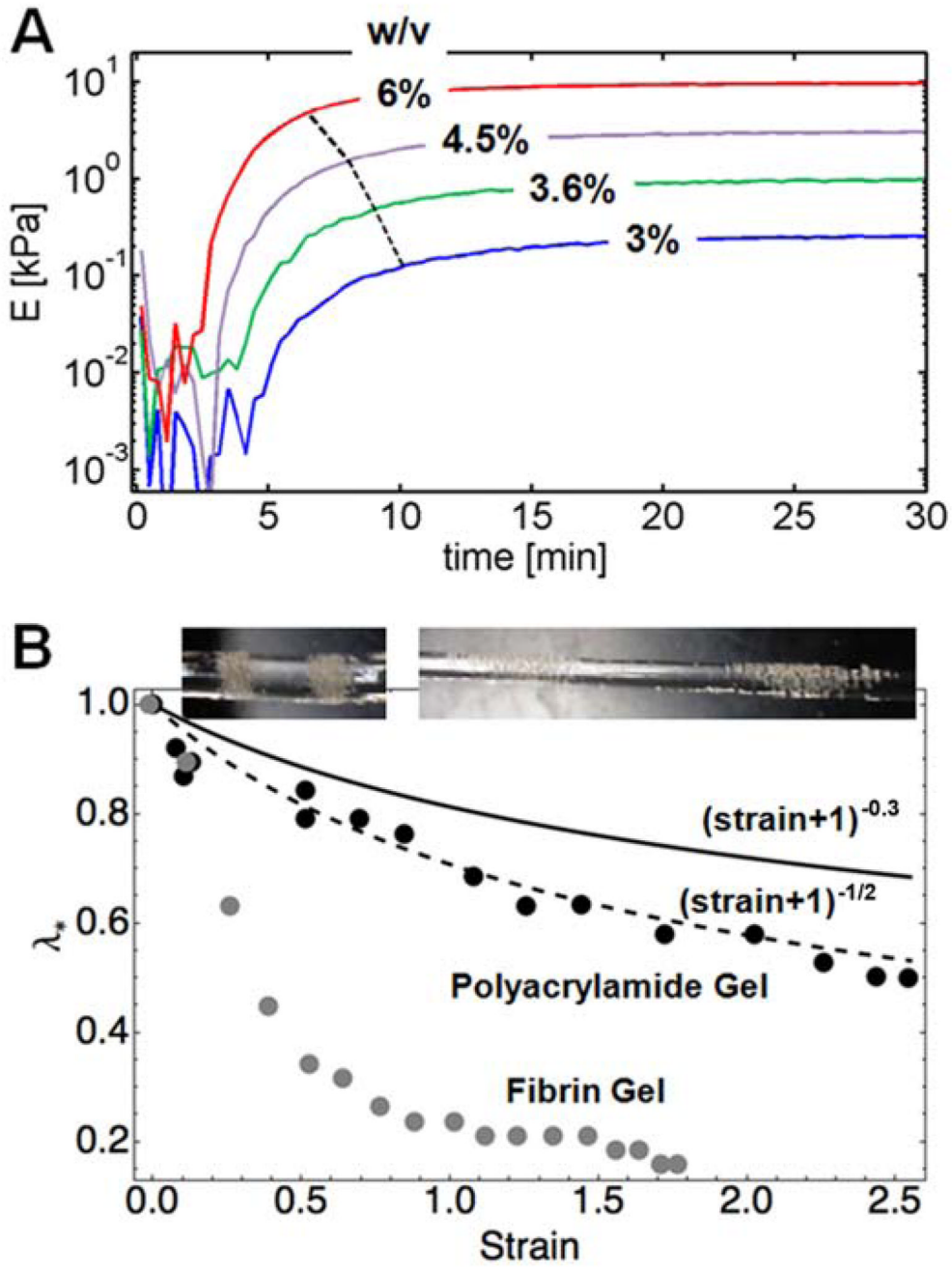

Figure 3.

Rheological characterization of PA gels. (A) Elasticity of PA gels was measured on a rheometer during gelation. Gel elasticity was controlled by varying acrylamide concentration from 3% to 6% w/v. Black dashed curve connects points of half-maximum stiffness, which illustrates faster polymerization in denser gels. (B) Cylindrical PA gels were stretched and simultaneously imaged to determine strain and relative width (λ_*). PA gels in air get thinner with stretch as $(\text{strain}+1)^{1/2}$ as expected for an incompressible material, implying a Poisson's ratio of 1/2 (black points, dashed line). For comparison, a compressible gel with $(\text{strain}+1)^{0.3}$ is shown as the solid line, and we also show data for networks of the ECM protein fibrin (gray points)

(26), with a width that decreases much faster with strain – corresponding to a negative compressibility that reflects protein unfolding.

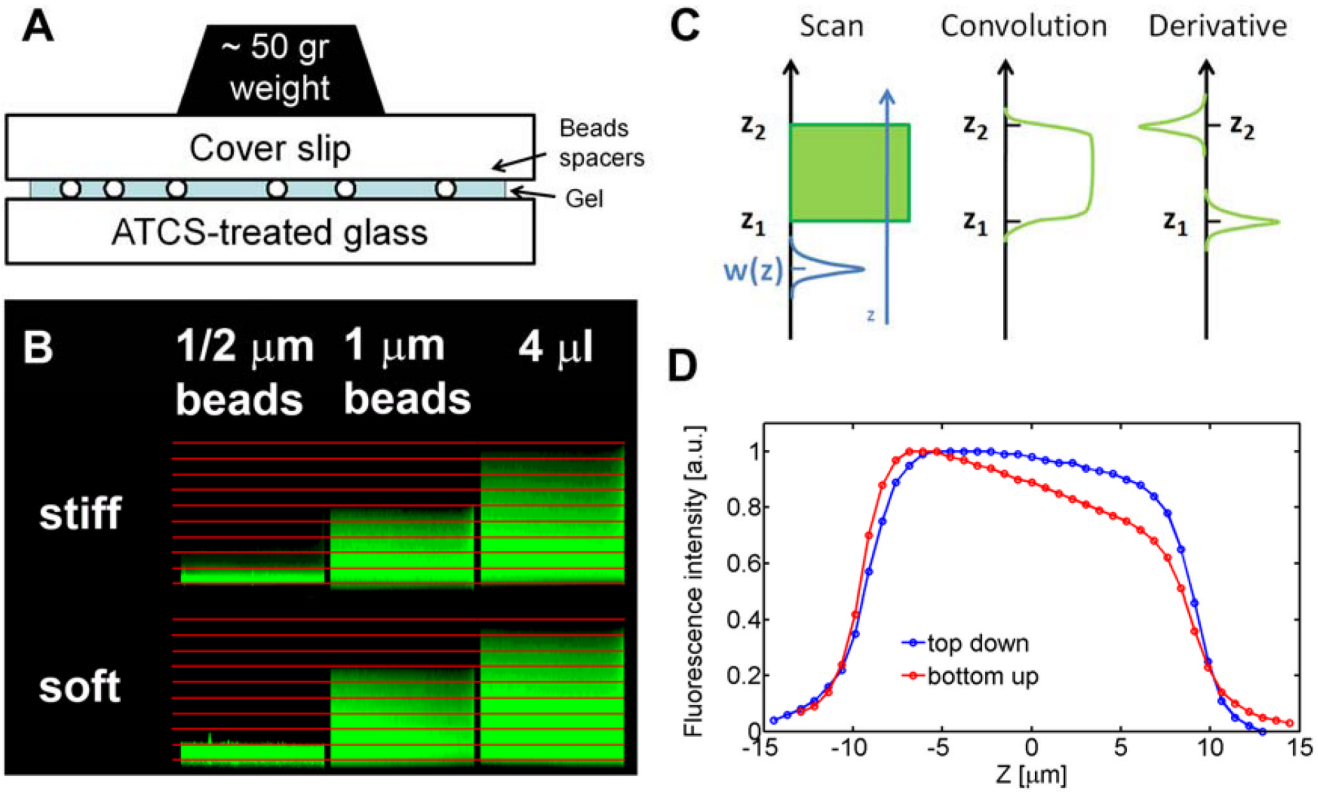

Figure 4.

Preparation of thin PA gels. (A) Thin PA gels were polymerized between an ATCS-treated coverslip and a clean coverslip. To control gel thickness, micron-scale bead spacers were included in the gels and pressed between the glass substrates using a weight. (B) Cross-sections of FITC-labeled gels were obtained using a laser scanning confocal microscope. The red grid indicates 2μm separation. (C) Gel thickness was evaluated using an edge detector, based on the peak centers of the z-dervative (right). (D) Fluorescence intensity profiles of a thick and soft gel were obtained by top-down and bottom-up laser scanning. Intensity profiles show decreasing intensity towards the gel top surface that becomes more prominent for the latter.

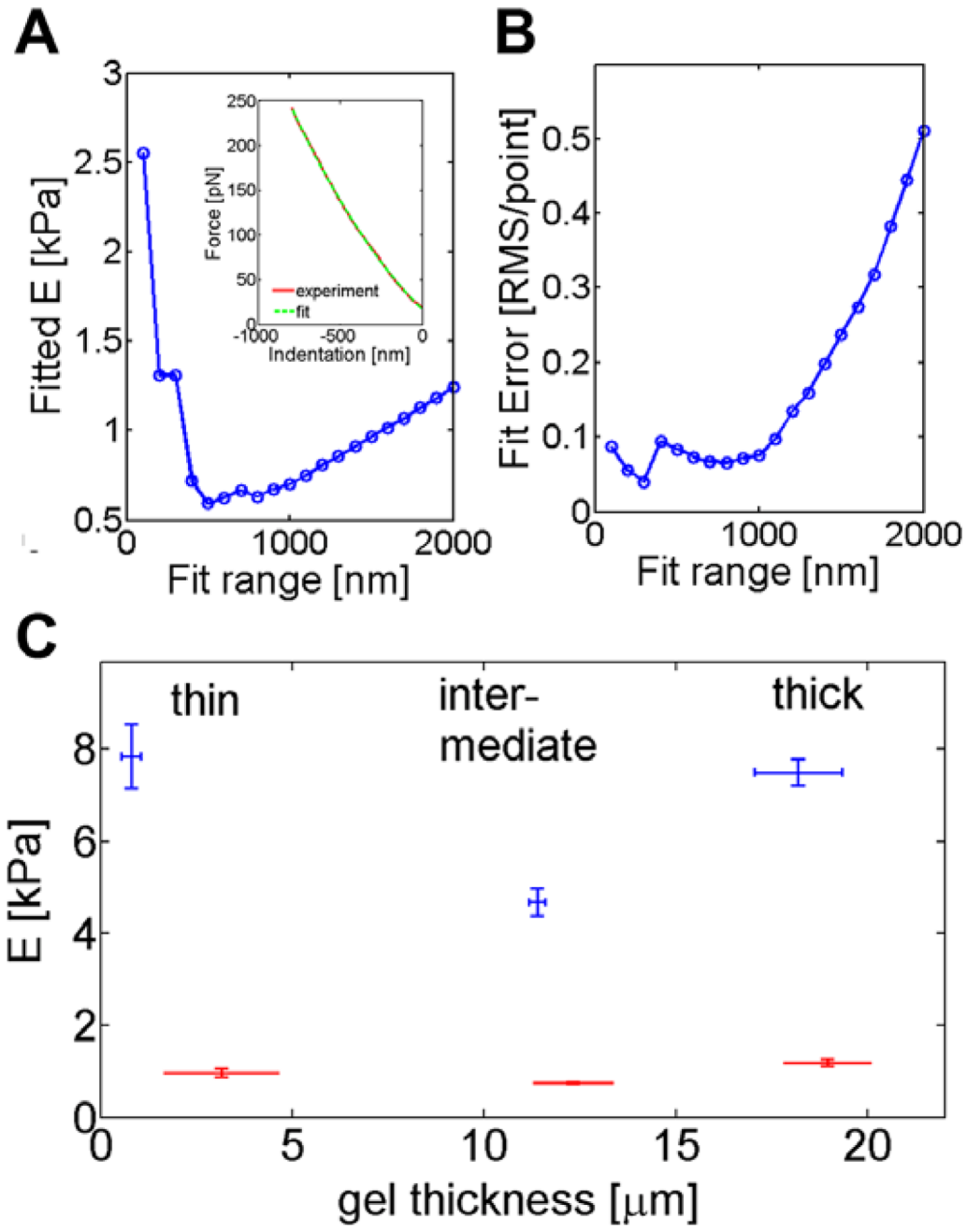

Figure 5.

Apparent elasticity of thin gels as evaluated from force-indentation analyses with AFM. (A) Force-indentation curves were fitted (inset) by a variant of the classical Hertz model adjusted for pyramidal (cone-like) tip geometry. (B) *E* was estimated in the constant-force regime which was robust to changes in fitting range (shown here between 500 nm and 1 μm). (C) The μ-elasticity of thin gels was higher than for intermediate thickness for both soft and stiff gels, indicative of the effective stiffening by the bottom rigid surface and with increased swelling of the intermediate-thickness gels.

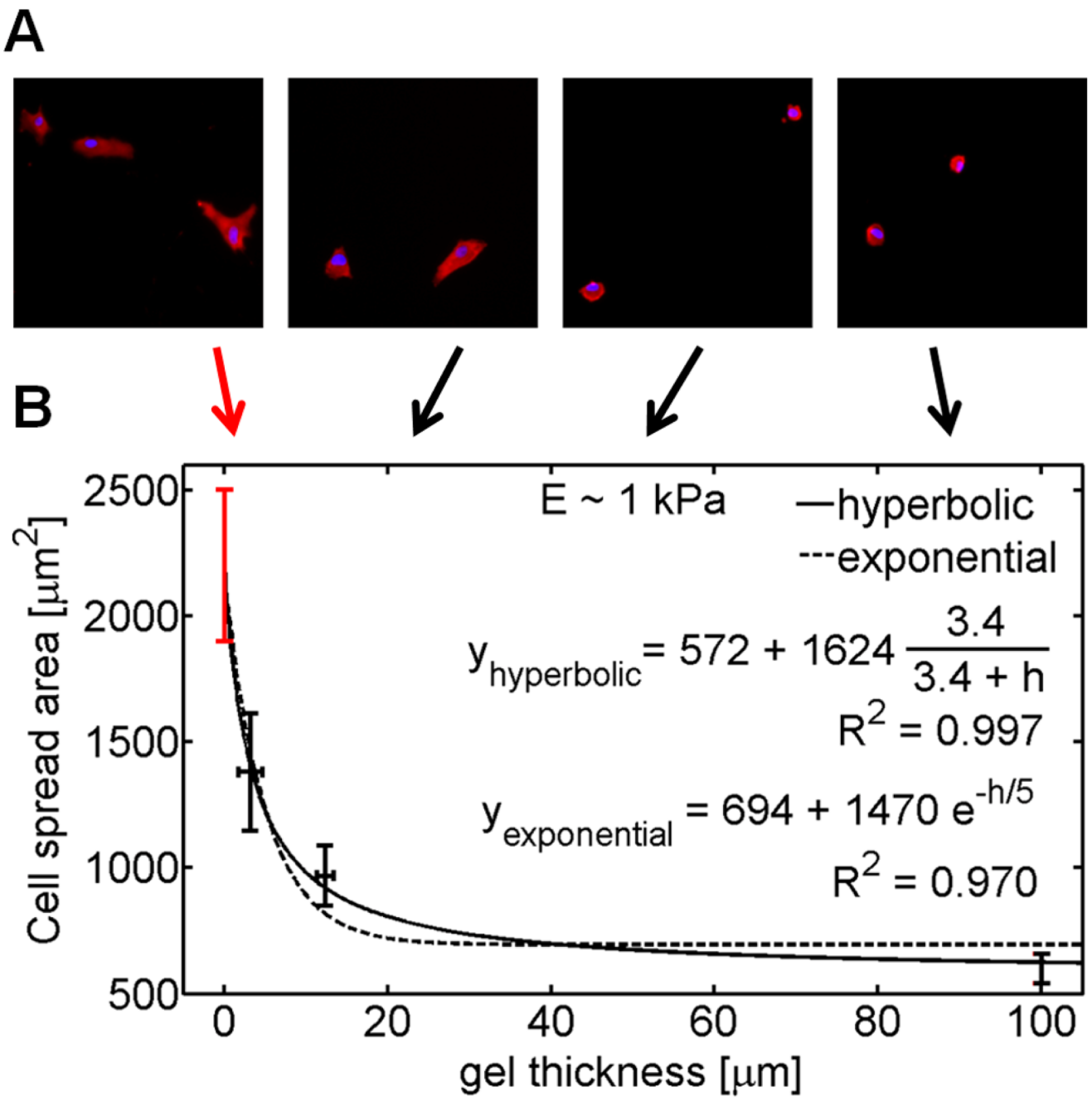

Figure 6.

How deeply do cells feel? (A) Mesenchymal stem cells were cultured on soft brain-like PA gels of varying thickness. The limit of zero gel thickness while maintain surface chemistry was mimicked using stiff (~34 kPa) collagen-coated PA gels, which have been shown to drive cell morphologies similar to collagen-coated rigid glass (red symbol). Cells were fixed after 24 hr in culture and labeled for actin (red) and DNA (blue). Cell spread area increased with decreasing gel thickness (B) Gel thickness at which MSCs begin to respond to the rigidity of the underlying glass substrate was estimated by a hyperbolic fit of the cell spread area. Compared to an exponential fit, the data was fit better with a hyperbolic relation, which yields 3.4 μm for how far cells feel(31).

Table 1

Thickness measurements for gels (±SEM).

Soft (3.6% w/v)	**h ± S.E. [μm]**	**swelling ratio**	**Stiff (6%w/v)**	**h ± S.E. [μm]**	**swelling ratio**
½ μm bead spacer	3.1 ± 1.5	6.2	**½ μm bead spacer**	0.8 ± 0.3	1.6
1 μm bead spacer	12.3 ± 1	12.3	**1 μm bead spacer**	11.4 ± 0.2	11.4
4 μl (no spacer)	18.9 ± 1.1	1.2*	**4 μl (no spacer)**	18.2 ± 1.1	1.2*

Soft gels swell more than the stiff gels, and the thickest gels (*) swelled the least. The swelling ratio for the latter was calculated by assuming a complete coverage of 18 mm diameter substrates with 4μl of fluid, which amounts to 15.7μm.

J Phys Condens Matter. Author manuscript; available in PMC 2011 May 19.